some better argument for the advantage to the herbivore, its failure to digest many algae appears to be a major adaptive inadequacy of the herbivore. This is possible, but it seems unlikely that the herbivore is truly blocked from selection of digestible foods or from development of mechanisms for digesting refractory foods.

Research (*13*) on the significance of undigested algae to the grazer has not dealt with the potential for photosynthetic activity during passage through the gut, probably because it would not be obvious that photosynthesis would proceed so effectively. Since active photosynthesis can occur in the gut, even for long periods, advantages may accrue to the herbivore by this route. Gases, photosynthate, or both, may be involved. Algae may be trading photosynthate to copepods in return for viable gut passage; this would imply coevolved mechanisms, including extraordinary release of photosynthate or important growth factors such as vitamins (*14*) by the cells and enzymatic selectivity by the herbivore to protect the algae. Gases are a second line of interaction. An internal oxygen pump of this magnitude opens possibilities for improved efficiency in food gathering and locomotion. Removal of CO_2 is also affected to the benefit of both herbivore and algae. Behavioral alteration of gut photosynthesis by adjustment of light climate during vertical migration is a potentially important by-product of algal-copepod coevolution.

ROBERT W. EPP
WILLIAM M. LEWIS, JR.
Environmental, Population, and Organismic Biology, University of Colorado, Boulder 80309

References and Notes

1. R. W. Epp and W. M. Lewis, Jr., *Ecology* **61**, 259 (1980).
2. Animals were obtained from University Pond on the campus of the University of Colorado, Boulder. All animals were acclimated to a temperature of 22.5°C in raw pond water for 24 hours before the experiments. Animals were fed on the natural assemblage of organisms in the pond, including an abundance of mixed phytoplankton. Copepodids were drawn at random from the last six developmental stages in the population.
3. R. W. Epp and W. M. Lewis, Jr., *Oecologia (Berlin)* **42**, 123 (1979).
4. The animals were observed under a microscope after anesthetization. Peristalsis of the gut continued after heavy anesthetization. Death was coincident with cessation of peristalsis. The test animals were all placed in fresh culture medium (medium without MS-222) after the experiments, and none showed vital signs.
5. Treatment was performed in total darkness or at a light intensity of 150 $\mu E\ m^{-2}\ sec^{-1}$ measured at the divers. This is approximately 7 percent of midday sunlight [R. J. List, Ed., *Smithsonian Meteorological Tables 1963* (Smithsonian Institution, Washington, D.C., ed. 6, 1963)]. All oxygen change experiments were conducted between 1200 and 1600 hours.
6. Metabolism of the control group was determined under normal laboratory illumination (< 50 $\mu E\ m^{-2}\ sec^{-1}$) on copepods starved for 24 hours before the experiment.
7. Metabolic rate per unit weight decreases with increasing body size in copepods (*1*) and most animals generally [C. L. Prosser, *Comparative Animal Physiology* (Saunders, Philadelphia, 1973)]. We first tested for the effect of size on metabolism. Body length was determined with an ocular micrometer. Length was then converted to weight by the equation of H. J. Dumont [*Oecologia (Berlin)* **19**, 75 (1975)]. Weights ranged from 1 to 13 μg (dry). We did not find a statistically significant effect of copepod size on metabolism of organisms in the gut. The typical effect of size on metabolism was significant in the control group, however. In our study, we need not consider size for any animals except the living controls; hence we can compare O_2 change per individual directly among experimental animals.
8. The normal retention time for food in the gut is only a few minutes during feeding periods [J. D. Green, *Oecologia (Berlin)* **21**, 345 (1975)]. A continual filtration is necessary for movement of material through the digestive system, however. Food appears to be retained in the gut for an extended time during periods of starvation (*13*).
9. R. J. Conover, in *Zoogeography and Diversity in Plankton*, S. van der Spoel and A. C. Pierrot-Bults, Eds. (Halsted, New York, 1979), p. 66.
10. The basal metabolic rate for the smallest copepodid that was used in this study (1.0 μg, dry weight) was 142 nl per individual per hour.
11. T. S. Ho and M. Alexander, *J. Phycol.* **10**, 95 (1974); C. M. Nadin-Hurley and A. Duncan, *Freshwater Biol.* **6**, 109 (1976).
12. G. S. Fryer, *J. Anim. Ecol.* **26**, 263 (1957).
13. K. G. Porter, *Am. Sci.* **65**, 159 (1977); *Science* **192**, 1332 (1976); *Verh. Int. Ver. Limnol.* **19**, 2840 (1975).
14. Copepods consume a significant amount of detritus [R. P. Gerber and N. Marshal, *Limnol. Oceanogr.* **19**, 815 (1974); S. A. Poulet, *Mar. Biol.* **34**, 117 (1976)], and they are apparently capable of digesting most particulate organic matter [P. Mayzaud and R. J. Conover, in *Tenth European Symposium on Marine Biology* (Ostend, Belgium, 1975), vol. 2, p. 415; J. Boucher, A. Laurec, J. F. Samain, S. L. Smith, in *ibid.*, p. 65]. Nevertheless, living organic matter is a dietary requirement. Conover (*9*) speculates that living organic matter may be a source of vitamins or other trace nutritional requirements. If this is the case, copepods may obtain an important nutritional supplement such as a vitamin while sequestering only a small fraction of the organic matter that is represented by the oxygen production.
15. We thank J. D. Allan and T. M. Frost for reviewing the manuscript and J. F. Saunders for identifying copepods. This work was supported by NSF grant DEB 8003883.

6 February 1981; revised 10 July 1981

Phase Locking, Period-Doubling Bifurcations, and Irregular Dynamics in Periodically Stimulated Cardiac Cells

Abstract. *The spontaneous rhythmic activity of aggregates of embryonic chick heart cells was perturbed by the injection of single current pulses and periodic trains of current pulses. The regular and irregular dynamics produced by periodic stimulation were predicted theoretically from a mathematical analysis of the response to single pulses. Period-doubling bifurcations, in which the period of a regular oscillation doubles, were predicted theoretically and observed experimentally.*

The phase of neural and cardiac oscillators can be reset by a single brief depolarizing or hyperpolarizing stimulus (*1–3*). Experimental determination of the dependence of the phase shift on the phase of the autonomous cycle at which the stimulus was delivered allows computation of a mathematical function called the Poincaré map (*4*). Analysis of the Poincaré map is carried out to predict the response to periodic stimulation (*1, 2, 4*). This work provides experimental confirmation of a recent theoretical prediction (*4*) that period-doubling bifurcations and irregular dynamics (*5*) should be observable in periodically stimulated oscillators.

The preparation has been described in detail (*6*). Briefly, apical portions of heart ventricles of 7-day-old embryonic chicks were dissociated into their component cells in 0.05 percent trypsin. The cells were transferred to a flask containing tissue culture medium (818A with a potassium concentration of 1.3 m*M*), which was placed on a gyratory shaker. Spheroidal aggregates (100 to 200 μm in diameter) of electrically coupled cells that beat spontaneously with a period between 0.4 and 1.3 seconds form after 48 to 72 hours of gyration. Experiments were performed on aggregates in the same culture medium at 35°C under a gas mixture of 5 percent CO_2, 10 percent O_2, and 85 percent N_2. Intracellular electrical recordings were made with glass microelectrodes filled with 3*M* KCl (resistance, 20 to 60 megohms). Current pulses were delivered through the same electrode and measured with a virtual ground circuit. Impalements were maintained for 2 to 5 hours. This report presents results for two aggregates out of ten studied.

Consider the response of an aggregate to a single current pulse delivered δ msec after the upstroke of the action potential (Fig. 1A). The length of the cycle immediately preceding the perturbation is called τ, and the phase ϕ of the cycle at which the stimulus was delivered is $\phi = \delta/\tau$, $0 \leq \phi < 1$. Control cycles with the phase labeled are shown in Fig. 1B. The cycle time of the perturbed cycle (the time from the upstroke immediately preceding the stimulus to the next upstroke) is called *T*. A stimulus was delivered after every ten beats, with δ increased by 10 msec each time. In Fig. 1C the normalized perturbed cycle length T/τ is plotted for two different preparations. In a single preparation, an increase

0036-8075/81/1218-1350$01.00/0

in stimulus intensity produces a transition from a continuous function such as that shown in Fig. 1C(i) to an apparently discontinuous function such as that shown in Fig. 1C(ii) (*7*).

Current pulses were periodically injected into the aggregate with period t_s ($100 \leq t_s \leq 700$ msec). For most t_s values in this range, phase-locked patterns result. A pattern is called an N:M phase-locked pattern if it is periodic in time and if for every N stimuli there are M action potentials, with action potentials occurring at M different times in the stimulus cycle. At first t_s was varied in 50-msec steps to sketch the boundaries of the

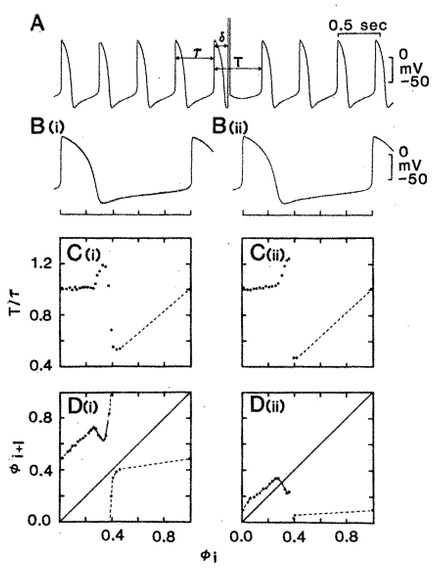

Fig. 1. (A) Transmembrane potential from an aggregate as a function of time, showing spontaneous electrical activity and effect of a 20-msec, 9-nA depolarizing pulse delivered at an interval of 160 msec following the action potential upstroke. The stimulus artifact is an off-scale vertical deflection following the fifth action potential. This early depolarizing stimulus prolongs the time at which the next action potential occurs. In (B to D), parts (ii) show results from this aggregate (aggregate 2), while parts (i) are from aggregate 1, taken from a different culture. (B) Membrane voltage as a function of phase ϕ, $0 \leq \phi < 1$. (C) Phase-resetting data, showing the normalized length T/τ of the perturbed cycle as a function of ϕ. (i) Pulse duration 40 msec, pulse amplitude 5 nA; (ii) pulse duration 20 msec, pulse amplitude 9 nA. For approximately $0.4 < \phi < 1.0$ the action potential upstroke occurs during the stimulus artifact and hence the perturbed cycle length cannot be exactly determined. The dashed line represents a linear interpolation that approximates the data. During collection of these data, the average control interbeat intervals (± 1 standard deviation) were (i) $\bar{\tau} = 515 \pm 5.7$ msec and (ii) $\bar{\tau} = 434 \pm 5.5$ msec. (D) Poincaré maps computed from Eq. 1 and the data in Fig. 1C; (i) $t_s = 250$ msec, (ii) $t_s = 480$ msec. The dashed line represents a linear interpolation used in iterating the Poincaré map; the solid line through the data points is a quartic fit for $0.22 < \phi_i < 0.37$.

major (2:1, 1:1, and 2:3) phase-locked regions. Then the intermediate regions were sampled by varying t_s in 10-msec steps. We first describe our experimental observations and then offer an interpretation based on an analysis of the Poincaré map.

Characteristic zones of regular and irregular dynamics were seen in both aggregates. Transitions occur at approximately the same values of $t_s/\bar{\tau}$, where $\bar{\tau}$ is the average control interbeat interval. For $0.55 < t_s/\bar{\tau} < 1.05$, 1:1 phase locking [Fig. 2A(ii)] is found. When t_s is decreased to $0.40 < t_s/\bar{\tau} < 0.55$ (zone α), dynamics analogous to the clinically observed Wenckebach phenomenon (*8*) are present. This phenomenon is characterized by a gradual prolongation of the time between a stimulus and the subsequent action potential until an action potential is skipped. This can occur in an irregular fashion (Fig. 2B) as well as in $m + 1$:m phase-locked patterns. As t_s is decreased below $0.4\,\bar{\tau}$, 2:1 phase locking is observed [Fig. 2A(i)].

For $1.05 < t_s/\bar{\tau} < 1.15$ (zone β), the ratio of stimulus frequency to action potential frequency is 1, but the stimulus no longer occurs at one fixed phase of the aggregate cycle as it does in 1:1 locking. Instead, the stimulus falls at two or more phases of the cycle. The dynamics in this narrow zone are highly variable and phase-locked patterns, when they exist, are typically not maintained for long stretches of time. For example, Fig. 2C(i) shows a transition from a 1:1 to a 2:2 phase-locked pattern which spontaneously occurred during stimulation with a fixed frequency. Similarly, brief stretches of 4:4 phase locking [Fig. 2C(ii)] and irregular dynamics [Fig. 2C(iii)] can both be observed at $t_s = 490$ msec. Such transitions may be due to slow drifts in the intrinsic frequency of the aggregate during stimulation.

For $1.15 < t_s/\bar{\tau} < 1.35$ (zone γ) there are irregular patterns with extra or interpolated beats (Fig. 2D). Further increase in t_s leads to a 2:3 phase-locked pattern [Fig. 2A(iii)].

As the stimulus strength increases, the widths of zones α and γ decrease. However, zone β is widest at intermediate stimulus strength. The two examples in this report were selected because there is a relatively broad β zone.

The experimentally derived curves shown in Fig. 1C can be used to predict the effects of periodic stimulation (*1, 2, 4*). If ϕ_i is the phase of the oscillator immediately before the ith stimulus, then

$$\phi_{i+1} = 1 - f(\phi_i) + \phi_i + \frac{t_s}{\bar{\tau}} \pmod 1 \qquad (1)$$

where $f(\phi)$ gives the normalized perturbed interbeat interval (T/τ) as a function of ϕ. The relation

$$\phi_{i+1} = g(\phi_i, t_s) \qquad (2)$$

defined by Eq. 1 is called the Poincaré map (Fig. 1D). For $t_s = 0$, the Poincaré map corresponds to the "new phase–old phase" phase-resetting curve, also called the phase transition curve (*1, 3, 4*). Starting from some initial phase ϕ_0, Eq. 1 can be iterated to compute the sequence of phases $\phi_0, \phi_1, \phi_2, \ldots$. If $\phi_N = \phi_0$ and $\phi_j \neq \phi_0$ for $0 < j < N$, then the Poincaré map has a cycle $\phi_0, \phi_1, \ldots, \phi_{N-1}, \phi_N = \phi_0$ of period N. If

$$\prod_{i=0}^{N-1} \left| \frac{\partial g}{\partial \phi} \right|_{\phi_i} < 1 \qquad (3)$$

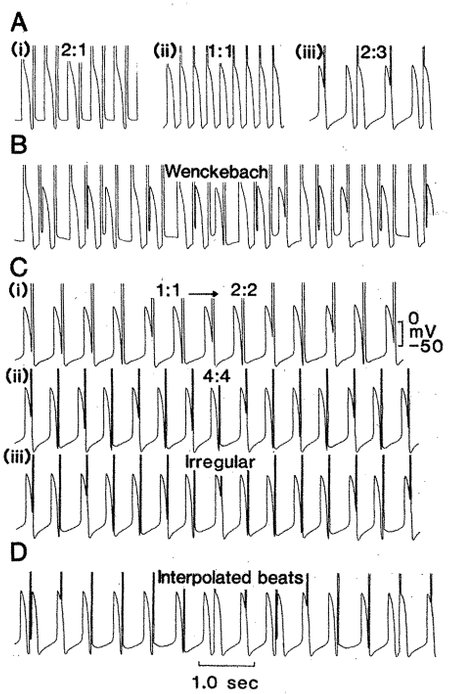

Fig. 2. Representative transmembrane recordings from both aggregates showing the effects of periodic stimulation with the same pulse durations and amplitudes as in Fig. 1C. (A) Stable phase-locked patterns: (i) 2:1 (aggregate 1, $t_s = 210$ msec); (ii) 1:1 (aggregate 2, $t_s = 240$ msec); (iii) 2:3 (aggregate 2, $t_s = 600$ msec). (B) Dynamics in zone α: irregular dynamics displaying the Wenckebach phenomenon (aggregate 1, $t_s = 280$ msec). (C) Dynamics in zone β: (i) 1:1 phase locking spontaneously changing to 2:2 phase locking (aggregate 1, $t_s = 550$ msec). During 2:2 phase locking there are two distinct phases of the cycle at which the stimuli fall. (ii) 4:4 phase locking (aggregate 2, $t_s = 490$ msec). There are four distinct phases of the cycle at which the stimuli fall. (iii) Irregular dynamics with one action potential in each stimulus cycle (aggregate 2, $t_s = 490$ msec). There is a narrow range of phases in which the stimuli fall. (D) Dynamics in zone γ: irregular dynamics displaying extra interpolated beats (aggregate 2, $t_s = 560$ msec).

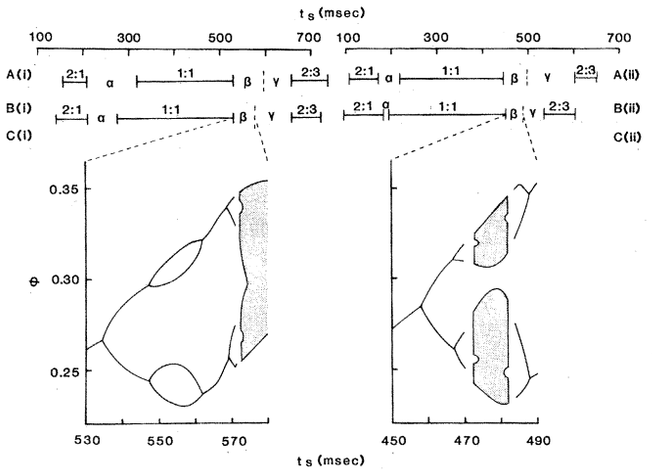

Fig. 3. Experimentally determined and theoretically computed dynamics. Parts (i) refer to aggregate 1, parts (ii) to aggregate 2. (A) Experimentally determined dynamics: there are three major phase-locking regions (2:1, 1:1, 2:3) and three zones of complicated dynamics labeled α, β, and γ (see text). (B) Theoretically predicted dynamics; note agreement with (A). (C) Theoretically predicted dynamics in zone β: curves give phase or phases in the cycle at which the stimuli fall during 1:1, 2:2, and 4:4 locking; stippled regions show the range of phases in which the stimulus falls during irregular dynamics.

then the period N cycle is stable, and the corresponding $N{:}M$ phase-locked pattern is stable with a period of Nt_s (*4*). A stable pattern is maintained despite small variations in either the oscillator itself or the stimulus parameters. The value of M is given by

$$M = \sum_{i=1}^{N} \left[1 - f(\phi_i) + \frac{t_s}{\bar{\tau}} \right] \qquad (4)$$

To iterate the Poincaré map, the function $f(\phi_i)$ in Eq. 1 was approximated by linear interpolation between the data points of Fig. 1C. There is close agreement (*9*) between the experimentally observed ranges of t_s that give simple phase-locked patterns (Fig. 3A) and those theoretically predicted from iteration of the Poincaré map (Fig. 3B). The Poincaré map also predicts the existence of irregular dynamics (dynamics that are not phase locked) in zones α, β, and γ. There are complex changes in the phase-locking patterns as t_s is changed within these zones. We explicitly compute these changes in zone β and briefly discuss the dynamics in the other two zones.

Numerical analysis of the Poincaré maps for t_s in zone β shows that for any ϕ_i in the interval (0.22, 0.37) all iterates of ϕ_i remain in this invariant interval. Moreover, this interval attracts iterates of ϕ_i for all ϕ_0 outside this interval. To determine the theoretically predicted dynamics in zone β, the Poincaré map in the invariant interval was fit to a quartic polynomial by a least-squares method. Numerical iteration of the Poincaré map in zone β shows a sequence of period-doubling bifurcations and irregular dynamics (Fig. 3C) as t_s is increased (*5*). In the zone of irregular dynamics, the phases of the stimuli are restricted to the shaded regions of Fig. 3C (*10*). The irregular dynamics result from a deterministic iterative process, with no added stochastic terms.

We do not experimentally observe all the bifurcations theoretically computed in Fig. 3C (*11*). However, we propose that the transition shown in Fig. 2C(i) from 1:1 phase locking (period of repeating pattern = 550 msec) to 2:2 phase locking (period of repeating pattern = 1100 msec) corresponds to the period-doubling bifurcation theoretically computed at $t_s \simeq 535$ msec [Fig. 3C(i)]. The 4:4 phase-locked pattern of Fig. 2C(ii) and the irregular dynamics of Fig. 2C(iii) provide further evidence for the correspondence between the experimental observations and the theoretical computations [Fig. 3C(ii)].

In zones α and γ complex behavior is also observed experimentally and predicted theoretically. For example, in zone α, the dynamics experimentally seen at t_s = 280 msec (Fig. 2B) are very similar to those predicted at t_s = 250 msec from the Poincaré map in Fig. 1D(i). The extra beats characteristic of zone γ (Fig. 2D) are also predicted.

This work has implications for the understanding of normal and pathologic behavior in cardiac tissue. The experimental work supports previous studies showing that periodically forced oscillators display phase-locked dynamics that are similar to clinically observed cardiac dysrhythmias (*2, 4, 12*). Moreover, the work suggests novel explanations for the genesis of 2:2 rhythms (*13*) and irregular dysrhythmias (*4*).

We have observed behavior that we propose arises as a consequence of period-doubling bifurcations in these experiments. Thus, exotic dynamic behavior that was previously seen in mathematical studies and in experiments in the physical sciences (*5*) may in general be present when biological oscillators are periodically perturbed.

MICHAEL R. GUEVARA
LEON GLASS, ALVIN SHRIER
Department of Physiology, McGill University, Montreal, Canada H3G 1Y6

References and Notes

1. D. H. Perkel, J. H. Schulman, T. H. Bullock, G. P. Moore, J. P. Segundo, *Science* **145**, 61 (1964); T. Pavlidis, *Biological Oscillators: Their Mathematical Analysis* (Academic Press, New York, 1973); H. M. Pinsker, *J. Neurophysiol.* **40**, 527 (1977); *ibid.*, p. 544.
2. G. K. Moe, J. Jalife, W. J. Mueller, B. Moe, *Circulation* **56**, 968 (1977); J. Jalife and G. K. Moe, *Am. J. Cardiol.* **43**, 761 (1979); S. Scott, thesis, State University of New York, Buffalo (1979).
3. A. T. Winfree, *Science* **197**, 761 (1977); *The Geometry of Biological Time* (Springer-Verlag, New York, 1980); J. Jalife and C. Antzelevitch, *Science* **206**, 695 (1979); T. Sano, T. Sawanobori, H. Adaniya, *Am. J. Physiol.* **235**, H379 (1978).
4. M. R. Guevara and L. Glass, *J. Math. Biol.*, in press.
5. A period-doubling bifurcation is the doubling of the period of an oscillation due to parametric changes. Period-doubling bifurcations and "chaotic" dynamics are observed in simple mathematical models and in experiments in the physical sciences: T. Y. Li and J. A. Yorke, *Am. Math. Mon.* **82**, 985 (1975); R. M. May, *Nature (London)* **261**, 459 (1976); M. C. Mackey and L. Glass, *Science* **197**, 287 (1977); J. P. Gollub, T. O. Brunner, B. G. Danly, *ibid.* **200**, 48 (1978); K. Tomita and T. Kai, *Prog. Theor. Phys. Suppl. 64* (1978), p. 280; R. H. G. Helleman, Ed., *Nonlinear Dynamics* (New York Academy of Sciences, New York, 1980); Editorial, *Phys. Today* **34**, 17 (March 1981).
6. R. L. DeHaan and L. J. DeFelice, *Theor. Chem.* **4**, 181 (1978); J. R. Clay and R. L. DeHaan, *Biophys. J.* **28**, 377 (1979); J. R. Clay and A. Shrier, *J. Physiol. (London)* **312**, 471 (1981).
7. There are many questions concerning the continuity properties of the graphs in Fig. 1, C and D. It is difficult to demonstrate experimentally that the points in Fig. 1C(ii) actually display a discontinuity. However, in this and many other preparations, repeated stimulation at the apparent discontinuity did not show evidence for intermediate values of T/τ. On theoretical grounds, discontinuities in the plots in Fig. 1C are expected [M. Kawato, *J. Math. Biol.* **12**, 13 (1981)]. However, the plots in Fig. 1D would not be expected to show discontinuities if one constructed the Poincaré map using the eventual phase [M. Kawato, cited above; E. N. Best, *Biophys. J.* **27**, 87 (1979)].
8. W. J. Mandel, Ed., *Cardiac Arrhythmias: Their Mechanisms, Diagnosis and Management* (Lippincott, Philadelphia, 1980).
9. There are many potential reasons for discrepancy between the predictions and experimental results. (i) The use of the Poincaré map is an approximation since it maps the state of a many-dimensional dynamical system to a single variable, the phase. (ii) The stimulation can lead to secondary electrophysiological changes in the aggregate such as changes in intrinsic frequency. (iii) There is beat-to-beat fluctuation in the autonomous cycle length in the absence of stimulation (*6*), and this "noise" tends to decrease the widths of the major stable phase-locked zones (compare Fig. 3A with Fig. 3B).
10. In the irregular region there are strong limitations on the phase at which the stimulus occurs. Compare Fig. 3C in this report with figure 3 in E. N. Lorenz, *Ann. N.Y. Acad. Sci.* **357**, 282 (1980).
11. "Noise" tends to destroy stable phase-locked patterns that either are complex or exist over very small ranges of t_s [L. Glass, C. Graves, G. A. Petrillo, M. C. Mackey, *J. Theor. Biol.* **86**, 455 (1980); J. P. Crutchfield and B. A. Huberman, *Phys. Lett.* **A77**, 407 (1980); R. Guttman, L. Feldman, E. Jakobsson, *J. Membr. Biol.* **56**, 9 (1980)]. Thus, there are fundamental limitations to the experimental observability of such patterns.

12. B. van der Pol and J. van der Mark, *Philos. Mag.* **6**, 763 (1928); S. D. Moulopoulos, N. Kardaras, D. A. Sideris, *Am. J. Physiol.* **208**, 154 (1965); J. V. O. Reid, *Am. Heart J.* **78**, 58 (1969); F. A. Roberge and R. A. Nadeau, *Can. J. Physiol. Pharmacol.* **42**, 695 (1969); D. A. Sideris and S. D. Moulopous, *J. Electrocardiol.* **10**, 51 (1977); C. R. Katholi, F. Urthaler, J. Macy, T. N. James, *Comp. Biomed. Res.* **10**, 529 (1977).
13. R. Langendorff, *Am. Heart J.* **55**, 181 (1958).
14. Supported by grants from the Canadian Heart Foundation and the Natural Sciences and Engineering Research Council of Canada. M.R.G. is a recipient of a predoctoral traineeship from the Canadian Heart Foundation. We thank D. Colizza for technical assistance and M. C. Mackey and A. T. Winfree for helpful conversations.

3 August 1981; revised 13 October 1981

Computer Averaging of Electron Micrographs of 40*S* Ribosomal Subunits

Abstract. *An enhanced lateral view of the 40S ribosomal subunit of HeLa cells has been obtained by computer averaging of single particles visualized in the electron microscope. Application of crystallographic criteria to independent averages shows that the reproducibility of the result is comparable to that obtained for thin, stained protein crystals by conventional Fourier filtration methods.*

Ribosomes are ribonucleoprotein particles that process the genetic information coded in messenger RNA (mRNA) for protein synthesis (*1*). Knowledge of their conformation is important for understanding their function in the assembly of polypeptide chains. Visualization by high-resolution electron microscopy offers obvious advantages for the study of the morphology of ribosomes. However, the large amount of noise in electron micrographs precludes detailed analysis, unless some method of image averaging (*2*, *3*) is employed. Studies of crystalline ribosome aggregates (*4*) have failed to give high-resolution structural information, because of the residual disorder in the arrangement of the ribosomes. We have used the computer to align and average large numbers of individual images corresponding to a single view of the ribosomal particle (*3*) for structural analysis of the small (40*S*) ribosomal subunit from HeLa cells [preliminary account in (*5*)].

Specimens for conventional transmission electron microscopy were prepared (*6*). A 0.5 percent aqueous uranyl acetate solution (not adjusted for *p*H) was used as contrasting stain. The grids were examined in an electron microscope (JEM 100B) operated at 80 kV, with a magnification of 70,000. The subunits (Fig. la) appear as elongate particles, approximately 250 by 130 Å, and display a strong preference for orientations referred to as right (R) and left (L) lateral views (*7*). The most characteristic structural feature is a beaklike protrusion (Fig. la, arrow).

Small areas containing particles in the L lateral view were selected from several electron micrographs and scanned into 128 by 128 arrays at 7.14 Å resolution. Each array was displayed on a computer-linked halftone monitor for interactive selection of a 64 by 64 window containing the particle (*8*).

A mask with a radius of 25 units (corresponding to 178 Å) was applied to each image to reduce the influence of noise in the further processing. Seventy-seven such masked arrays were aligned (Fig. 1b) by using auto- and cross-correlation functions (*3*, *9*), with one particle selected as reference. The reference particle was low-pass filtered (see Fig. 2b, legend) to a resolution of 1/28 $Å^{-1}$ to eliminate high-resolution portions of the noise. After the first alignment pass, the alignment was refined in two cycles, with the average of the previous cycle used as reference each time.

The first pass aligned the particles to within a few degrees of the reference. This approximate positioning allowed use of the direct method of orientation search (*10*) in the subsequent refinement cycles, in which the image, rather than its autocorrelation function, was subjected to the rotational cross-correlation. The combination of autocorrelation (*9*) and direct (*10*) methods was found to give a higher reproducible resolution in the final average than was given by the autocorrelation method alone.

The average of 77 aligned images (Fig. 2, a and b) shows the 40*S* subunit to have a complex morphology. It appears to be divided by stain incursions into three major regions, each characterized by three prominent minima in stain density.

Several different methods were used to ascertain the validity of the result: comparison of independent averages, analysis of the variance associated with

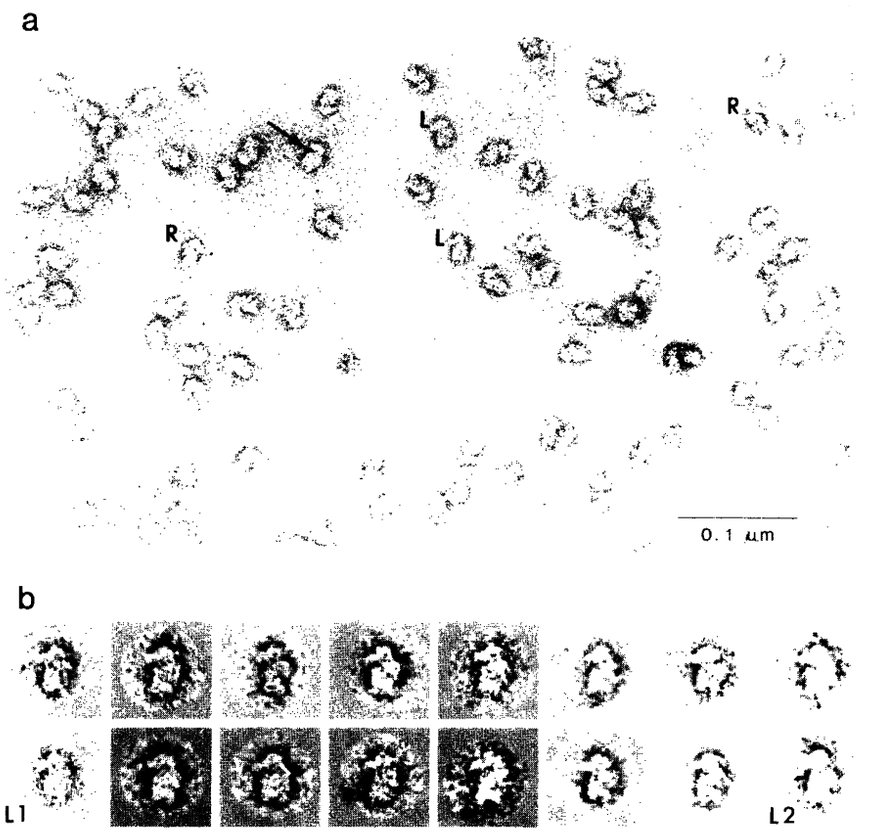

Fig. 1. (a) Electron micrograph showing left-oriented (L) and right-oriented (R) lateral views of 40*S* ribosomal subunits of HeLa cells. The particles in L views were selected for processing. Arrow points to the characteristic beaklike protrusion. (b) Gallery showing 16 of the 77 particles after alignment. L1 and L2 were used as the initial reference particles in the alignments.

0036-8075/81/1218-1353$01.00/0